RESEARCH ARTICLE

Thermoelectric Materials

Energy & Environmental Materials WILEY

# Designing Spin-Crossover Systems to Enhance Thermopower and Thermoelectric Figure-of-Merit in Paramagnetic Materials

*Md Mobarak Hossain Polash, Matthew Stone, Songxue Chi, and Daryoosh Vashaee**

**Thermoelectric materials, capable of converting temperature gradients into electrical power, have been traditionally limited by a trade-off between thermopower and electrical conductivity. This study introduces a novel, broadly applicable approach that enhances both the spin-driven thermopower and the thermoelectric figure-of-merit (zT) without compromising electrical conductivity, using temperature-driven spin crossover. Our approach, supported by both theoretical and experimental evidence, is demonstrated through a case study of chromium doped-manganese telluride, but is not confined to this material and can be extended to other magnetic materials. By introducing dopants to create a high crystal field and exploiting the entropy changes associated with temperature-driven spin crossover, we achieved a significant increase in thermopower, by approximately 136 μV $K^{-1}$, representing more than a 200% enhancement at elevated temperatures within the paramagnetic domain. Our exploration of the bipolar semiconducting nature of these materials reveals that suppressing bipolar magnon/paramagnon-drag thermopower is key to understanding and utilizing spin crossover-driven thermopower. These findings, validated by inelastic neutron scattering, X-ray photoemission spectroscopy, thermal transport, and energy conversion measurements, shed light on crucial material design parameters. We provide a comprehensive framework that analyzes the interplay between spin entropy, hopping transport, and magnon/paramagnon lifetimes, paving the way for the development of high-performance spin-driven thermoelectric materials.**

## 1. Introduction

Thermoelectric materials have the potential to convert waste heat into electricity, offering a sustainable energy solution. However, their efficiency is often limited by a fundamental trade-off between thermopower and electrical conductivity. Recent advances in spin-caloritronics have highlighted the role of paramagnetic (PM) effects, including spin entropy,[1–3] superparamagnetism,[4,5] spin fluctuations,[6,7] and paramagnon-drag,[8,9] in enhancing thermoelectric performance. These effects have garnered significant interest in both disordered PM semiconductors and magnetic semiconductors as promising candidates for high-performance thermoelectric materials.

Among the various magnetic semiconductors, antiferromagnetic (AFM) semiconductors have been widely studied for their thermoelectric applications.[10–12] They are favored over their ferromagnetic (FM) counterparts due to the presence of doubly degenerate magnon bands, higher magnon group velocities, and longer magnon lifetimes. These properties are crucial for the transport of thermal energy and charge carriers in thermoelectric materials.[8]

In the condensed matter environment, charge carrier spins, spin-waves (magnons), spin-wave packets (paramagnons), and spin entropy from spin and configurational degeneracies can exhibit unique thermoelectric transport properties under the influence of doping, nano-inclusion, and external fields.[1–15] While most spin-caloritronic effects are present only in magnetically ordered domains below the transition temperatures, paramagnon-drag and spin entropy can exist in disordered paramagnetic domains, leading to significant improvements in thermopower.

In the realm of PM phases, paramagnons play a crucial role. Paramagnons are quantized spin-wave packets that exist within short to mid-range magnetic order in PM phases.[16] They are capable of dragging itinerant (or band) carriers through mutual coupling, in addition to the conventional diffusion transport mechanism (see **Figure** 1a–c).[8,9] This interaction between carriers and paramagnons can significantly enhance thermopower, as has been demonstrated in recent studies of AFM Li-doped MnTe[8] and FM Heusler alloys.[6] However, the magnon and paramagnon-drag thermopower can be significantly affected by the bipolar conduction nature.[17]

Furthermore, the concept of spin entropy, which arises from the spin and orbital degeneracies of localized ions, has been shown to enhance thermopower in strongly correlated materials.[1–3] The electronic spin entropy is influenced by the competition between the

Dr. M. M. H. Polash, Prof. D. Vashaee
Department of Materials Science and Engineering, NC State University, Raleigh, North Carolina 27606, USA
E-mail: dvashae@ncsu.edu
Dr. M. Stone, Dr. S. Chi
Neutron Scattering Division, Oak Ridge National Laboratory, Oak Ridge, Tennessee 37831, USA
The ORCID identification number(s) for the author(s) of this article can be found under https://doi.org/10.1002/eem2.12822.

**DOI: 10.1002/eem2.12822**

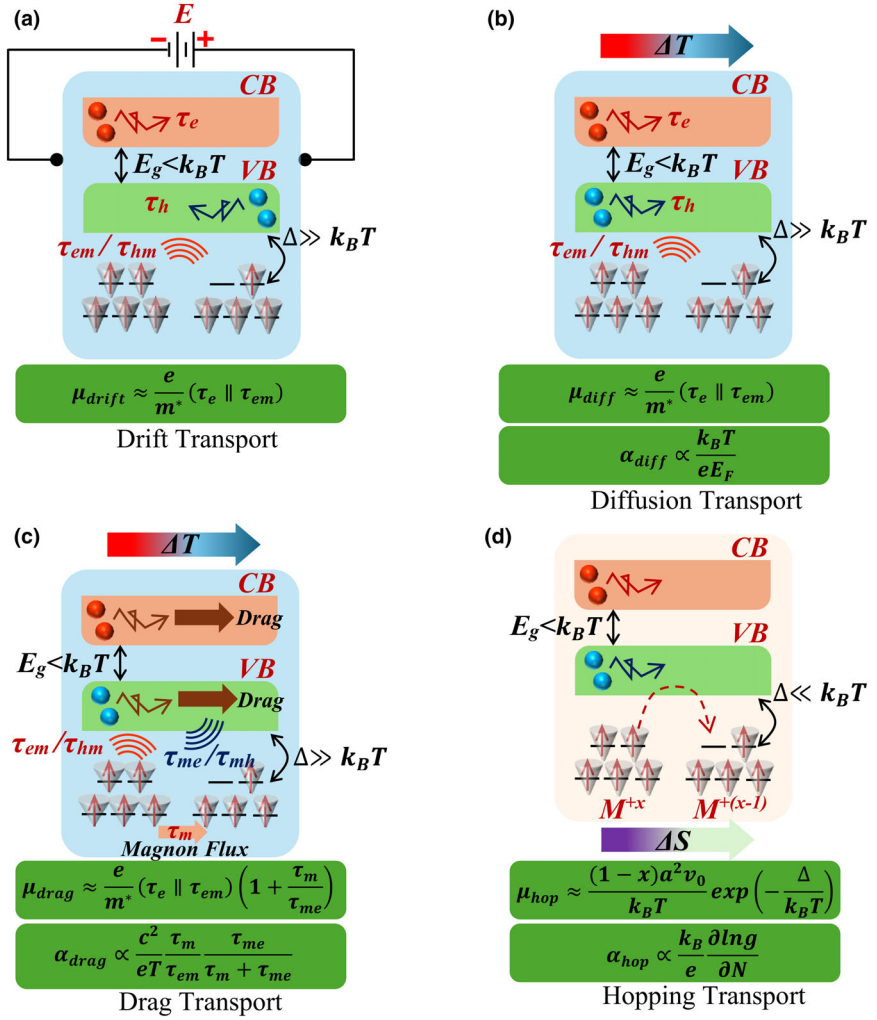


**Figure 1.** Carrier transport processes in magnetic and paramagnetic semiconductors: This figure illustrates various carrier transport mechanisms in magnetic or paramagnetic semiconductors, along with their respective mobility ($\mu$) and thermopower ($\alpha$) expressions: a) Drift Transport: Band carriers are driven by an external electric field ($E$), moving electrons and holes in opposite directions. This process is dominated by Coulomb scattering, carrier-phonon relaxations ($\tau_e$ or $\tau_h$), and carrier-magnon scattering ($\tau_{em}$ or $\tau_{hm}$), the latter due to s-d exchange interactions. b) Diffusion Transport: A temperature gradient ($\Delta T$) drives band carriers in the same direction as the gradient, facilitating electron and hole movement. c) Drag Transport: Band carriers are propelled by a magnon flux, created by a temperature gradient, due to magnon/paramagnon-carrier drag, characterized by $\tau_{em}$ or $\tau_{hm}$, $\tau_{me}$ or $\tau_{mh}$, and $\tau_m$ (magnon/paramagnon lifetime). d) Hopping Transport: Localized carriers engage in hopping transport due to an entropy difference ($\Delta S$) arising from spin and orbital degrees of freedom. This transport is initiated when thermal energy ($k_BT$) exceeds the activation energy ($\Delta$) and is dependent on the distance between hopping centers a), the availability of centers (1-$x$), and the hopping frequency ($\nu_0$). CB denotes the conduction band, VB the valence band, $E_g$ the bandgap, $E_F$ the Fermi energy, $e$ the electron charge, $m^*$ the effective mass, $c$ the magnon velocity, $g$ the total degeneracy, and $N$ the total number of particles.

crystalline field and Hund's rule coupling[1–3] leading to hopping transport in localized carriers that is governed by the spin-selection rule (see Figure 1d).[18] The mobility of these carriers is determined by various factors, including activation energy, hopping frequency, separation between hopping centers, and configurational degeneracy.[19]

While the net paramagnon-drag thermopower can be significantly reduced by the bipolar conduction, spin entropy thermopower is not similarly affected. This makes spin entropy a potentially effective route for achieving high thermoelectric performance in bipolar thermoelectric materials. However, despite the promising prospects of spin entropy, high thermoelectric performance resulting from this effect is rarely reported in materials with either intrinsic or extrinsic carrier nature.

In this study, we demonstrate high thermoelectric performance in Chromium (Cr)-doped Manganese Telluride (MnTe). We will discuss how, in this bipolar ferromagnetic system, the enhanced spin entropy resulting from temperature-driven spin-crossover plays a crucial role. Spin-crossover is a phenomenon where a gradual temperature-driven transition occurs between high-spin and low-spin states.[20] To provide an overview of the objectives and findings of this work, we have summarized contemporary studies on MnTe-based thermoelectrics in Table 1. The rest of the paper will discuss the details of our study.

The thermoelectric performance of magnetic semiconductors can be enhanced by designing their spin environment, which directly influences spin-driven thermoelectric effects. However, this approach has been infrequently explored in previous studies.[24–26] The spin nature of these materials can be modified, for example, through temperature-driven spin-crossover, which transitions the spin states and impacts the corresponding properties of the magnetic or paramagnetic materials.

Our research demonstrates an enhancement of PM spin-caloritronic effects due to spin-crossover in Cr-doped MnTe. We investigate its impact on carrier and thermoelectric transport properties and aim to understand the underlying processes to achieve high thermoelectric performance.

Recent studies have reported that transition metal doping, specifically with chromium (Cr), in MnTe can exhibit several unique properties. These include magnon bipolar carrier drag,[17] crystal field-induced low-spin (LS) state in manganese (Mn) ions,[17] presence of $Mn^{3+}$ ions due to charge-transfer reactions,[17] spin-crossover mediated heat capacity contribution,[27] FM natures in AFM host,[17,27] and magnon lifetime independent drag thermopower.[17]

Cr-doped MnTe exhibits a bipolar carrier nature due to the substitution of $Mn^{2+}$ by $Cr^{3+}$, FM-AFM clustering due to the presence of FM CrTe phase, and a temperature-driven spin-crossover in the 450–750 K range.[17,27] The high crystal field from $Cr^{3+}$ ions induces LS states in Mn ions, which transition to the high-spin (HS) state above 450 K as thermal energy overcomes the crystal field.[27] In Cr-doped MnTe, both $Mn^{3+}$ ($3d^4$) and $Cr^{2+}$ ($3d^4$) ions can exist along with $Mn^{2+}$ ($3d^5$) and $Cr^{3+}$ ($3d^3$) due to the electron transfer reaction: $Mn^{2+} + Cr^{3+} \rightarrow Mn^{3+} + Cr^{2+}$.[17,27] The

**Table 1.** Recently studied MnTe-based spin-caloritronic systems.

| Material system | Conduction type | Spin-caloritronic effect | Impacted thermoelectric properties | References |
|---|---|---|---|---|
| MnTe | p-Type | Magnon-drag effect | Significant enhancement in thermopower up to the magnetic transition temperature | [21] |
| MnTe:Li | p-Type | Paramagnon-drag effect | Linear enhancement in thermopower in the paramagnetic domain | [8] |
| | | Spin Entropy | Thermopower enhancement due to spin entropy delocalized d-electrons | [22] |
| GeMnTe2 | p-Type | Spin thermodynamic entropy | Thermopower enhancement from disordering of spin orientation by modifying band hybridization | [23] |
| MnTe:Cr | Bipolar | Magnon bipolar carrier-drag effect | Suppression of magnon/paramagnon-drag effect below and above the transition temperature | [17] |
| | | Spin-crossover effect | Thermopower enhancement at deep paramagnetic temperature due to low spin to high spin state transition of magnetic ions from thermal energy higher than crystal field energy | [27], this work |

magnetic susceptibility measurement reveals the LS (spin number, $S = 0.5$) to HS ($S = 2.4$) transition of Mn ions at high temperatures in the PM regime (above the Curie temperature of $T_C \sim 280$ K),[27] which supports the enhancement of the spin entropy. The heat capacity trend of Cr-doped MnTe indicates the presence of magnons and paramagnons, which can be influenced by the temperature-driven spin-crossover.[17,27]

The impact of spin-crossover on paramagnon lifetime is investigated with inelastic neutron scattering (INS) and found to have insignificant variation in the spin-crossover temperature range. Therefore, a detailed analysis is performed to illustrate and analyze the impact of spin-crossover on different carrier transport processes. Understanding these processes will be instrumental in designing future high-performance magnetic or PM thermoelectric materials.

## 2. Results

**Figure 2** summarizes the thermoelectric transport properties of 5% Cr-doped MnTe including electrical conductivity ($\sigma$) and thermopower ($\alpha$). The thermal conductivity ($\kappa$) and $zT = \sigma\alpha^2/\kappa$ are given in the File S1. For better understanding, electrical conductivity and thermopower of MnTe and Li-doped MnTe are shown in the insets. MnTe is a p-type semiconductor that shows an extrinsic to intrinsic transition in conductivity at Néel temperature due to spin-disorder scattering.[17] Li-doped MnTe has higher p-type conductivity due to the substitution of $Mn^{2+}$ ions by $Li^{+}$ ions causing the creation of holes (see Equation 1). Li-doped MnTe also shows similar extrinsic to intrinsic transition in conductivity at Néel temperature like MnTe. It is also known that Cr-doping reduces the bandgap of MnTe,[17,27] and compensates the p-type conductivity by substituting the $Mn^{2+}$ ions with electron donor $Cr^{3+}$ ions that introduce the intrinsic carrier nature (see Equation 2). Here, 3+ is the stable oxidation state of Cr in this material system. The hole and electron donor nature of Li and Cr-doping in MnTe, respectively, can be understood from the defect reaction equations considering the conservation of mass, charge, and sites based on Kroger-Vink notation:

$$Mn_{0.97}Li_{0.03}Te \rightarrow 0.03Li_{Mn}^{-} + 0.95Mn_{Mn}^{\times} + Te_{Te}^{\times} + 0.03h^{+} \quad (1)$$

$$Mn_{0.95}Cr_{0.05}Te \rightarrow 0.05Cr_{Mn}^{+} + 0.95Mn_{Mn}^{\times} + Te_{Te}^{\times} + 0.05e^{-} \quad (2)$$

Here, $X_Y$ indicates X ions substituting Y ions, and the net charge of the $X_Y$ site is obtained by subtracting the charge of Y from the charge of X. For example, at the $Li_{Mn}$ site, the net charge is $(+1) - (+2) = -1$. The number of holes/electrons is obtained such that the right side of the equation is charge neutral.

Based on the electrical conductivity trend of Cr-doped MnTe shown in Figure 2a, we can observe two distinct types of conductivity. Below 500 K, the electrical conductivity increases with temperature due to thermal carrier excitation. Above approximately 500 K, electrical conductivity exhibits an enhancement that can be attributed to additional spin-crossover mediated carrier hopping. It is important to note that this hopping conduction occurs at a deep paramagnetic temperature ($T_C \sim 280$ K), where no crystal or magnetic structure change is observed,[27] and consequently, no band structure change occurs.

In **Figure 3a**, the diffusion and hopping electrical conductivities are extracted, assuming that the conductivity below 500 K primarily results from the bipolar diffusion of thermally excited carriers. Above the transition temperature, the mobility of conduction carriers in the MnTe system typically reaches a saturation point due to the saturation of spin disorder scattering.[8,17] Therefore, the diffusion electrical conductivity above the transition temperature follows the trend of carrier concentration, which exhibits an exponential thermal excitation trend.[17] In contrast, the hopping conductivity, which is associated with the transport of localized carriers, primarily follows the hopping mobility trend, as the number of localized carriers remains approximately constant. Based on these considerations, the hopping mobility is estimated and presented in Figure 3a. The hopping mobility is significantly lower than the typical diffusion mobility of conduction carriers in the MnTe system.[8,17] According to the hopping mobility expression shown in Figure 1, the hopping barrier is determined to be 1.21 eV, and the hopping frequency is found to be in the range of 1 MHz. As indicated in Figure 3, the hopping transport commences at temperatures above approximately 500 K, and the anomalous enhancements of thermopower and inverse magnetic susceptibility also occur at a similar temperature range.

According to Figures 2b and 3b, the total thermopower of Cr-doped MnTe is nearly zero below its Curie temperature ($T_C \sim 280$ K), then experiences a slight increase until 500 K, and shows a significant enhancement above 500 K, within a deep paramagnetic regime. In

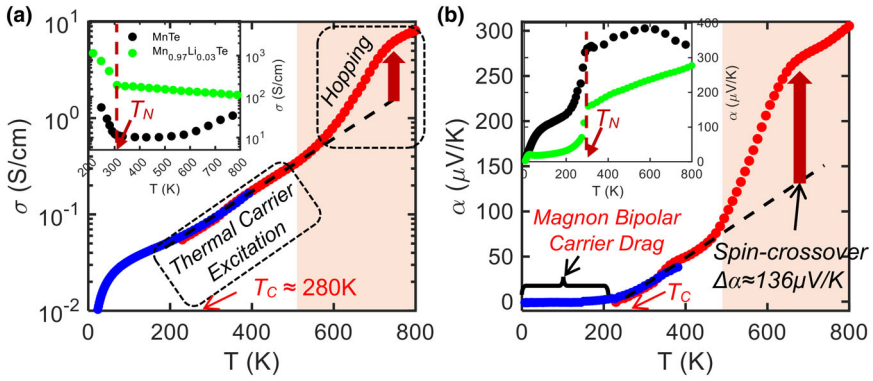


**Figure 2.** Temperature-dependent thermoelectric transport properties of 5% Cr-doped MnTe: This figure presents the thermoelectric transport properties of 5% Cr-doped MnTe, which has a Curie temperature ($T_C$) of approximately 280 K. a) Electrical Conductivity: The distinct regions of thermal carrier excitation and hopping conduction as functions of temperature. b) Thermopower: The contributions of magnon bipolar carrier drag and spin-crossover mediated spin-entropy to thermopower, again as functions of temperature. In both graphs, low-temperature data (blue circles) were obtained using a Physical Property Measurement System (PPMS), while high-temperature data (red circles) were collected using standard thermoelectric property measuring equipment, as described in the Methods section. The insets show the electrical conductivity (left) and thermopower (right) of pure MnTe (black circles) and Li-doped MnTe (green circles) for comparison.

contrast, both MnTe and Li-doped MnTe exhibit an exponential increase in thermopower below their Néel temperatures and a linear improvement above the Néel temperature due to magnon and paramagnon-drag effects, respectively. Given that Cr-doped MnTe exhibits a bipolar conduction nature (as evidenced by Hall data in reference 17), the thermopower (including both electronic and drag contributions) below the Curie temperature is significantly reduced, primarily due to the bipolar effect on diffusion and magnon carrier drag transport.[17]

Above the Curie temperature ($T_C \sim 280$ K), thermopower begins to incrementally increase with temperature, with an abnormal rise of approximately 136 $\mu V\,K^{-1}$ above 500 K, deep within the paramagnetic domain. Recent studies suggest that this behavior may be linked to phenomena such as paramagnon drag effect and spin entropy.[8,22,28] It is imperative to elucidate the anomalous thermopower enhancement above 500 K by examining these contributing factors. Specifically, if paramagnon drag is influencing the paramagnetic thermopower trend in Cr-doped MnTe, the observed thermopower spike should correlate with an increase in paramagnon lifetime at similar temperatures, given that drag thermopower is directly proportional to paramagnon lifetime.[8,28] Our measurements of paramagnon lifetime at elevated temperatures aim to test this hypothesis, with details provided in the subsequent discussion.

To substantiate the role of spin entropy in thermopower, it is necessary to confirm the presence of various magnetic ions in Cr-doped MnTe and to demonstrate an increase in entropy at the pertinent temperatures. The experimental evidence supporting these assertions is outlined below. In summary, spin entropy appears to underpin the thermopower trends in Cr-doped MnTe, a topic that will be further explored in the following section.

To affirm the influence of paramagnon drag on the paramagnetic thermopower of Cr-doped MnTe, an analysis of heat capacity data is instructive, as it reflects the presence of magnons and paramagnons. Prior literature has documented heat capacity measurements for Cr-doped MnTe, verifying the existence of these quasiparticles.[17,27]

While the bipolar effect markedly diminishes magnon drag thermopower below the Curie temperature,[17] a residual paramagnon drag thermopower persists, albeit reduced. It is important to note that the extent of this suppression can vary based on multiple factors,[17] including magnon/paramagnon lifetime, which may be altered by magnetic transitions.

To corroborate the anomalous thermopower enhancement in the deep paramagnetic regime, we have undertaken measurements of paramagnon lifetime in Cr-doped MnTe to detect any variations within this regime. Literature indicates that Cr-doped MnTe undergoes a spin-state transition at deep paramagnetic temperatures,[27] hence measuring paramagnon lifetime can provide insights into the potential interplay between paramagnons and spin-state transitions. Accordingly, we have conducted INS measurements across a temperature range of 50–800 K. The paramagnon lifetime is derived from the energy-momentum spectra obtained from these INS measurements.

The INS spectra for Cr-doped MnTe, depicted in **Figure** 4a–f, represent selected temperatures within the magnetic and PM domains, with additional spectra available in the File S1. As shown in Figure 4a, the low-temperature INS data (<290 K) mirrors the magnon dispersion observed in Li-doped MnTe,[8] attributable to the influence of $Mn^{2+}$ ions on the spin-wave nature of both MnTe systems. The orientation-averaged magnon branches in polycrystalline Cr-doped MnTe originate from magnon Bragg peaks at approximately 0.92 and 1.95 $Å^{-1}$, with magnon bands extending to ~30 meV. Notably, distinct magnon branches are present at 290 K, just above the $T_C$, suggesting that Mn ions predominate in the magnon system of Cr-doped MnTe, with the FM character stemming from Cr-induced impurity domains within the MnTe matrix. Beyond 290 K, the magnon bands at 30 meV vanish, as detailed in the File S1, and paramagnon scattering emerges near 0.92 $Å^{-1}$. The lifetimes of magnons and paramagnons are ascertained from the Lorentzian-fitted broad inelastic features, S(E), also known as quasi-elastic, which manifest at $E = 0$ for the PM domain and $E > 10$ meV for the magnetic domain, in accordance with the Heisenberg uncertainty principle (refer to Figure 4g,h). The paramagnon scattering feature maintains a consistent intensity and energy distribution across all temperatures within the PM domain. Paramagnon lifetimes are calculated from the S(E) profile at 0.92 $Å^{-1}$, while magnon lifetimes are derived from the S(E) at 1.5 $Å^{-1}$.

Figure 4i presents the estimated lifetimes of magnons and paramagnons. Typically, paramagnon lifetime estimations are more accurate than those of magnons. Instrumental limitations often result in underestimations of the actual magnon lifetime. Above approximately 300 K, the paramagnon lifetime remains nearly constant at around 24 fs, closely aligning with the measured paramagnon lifetime of 27 fs in Li-doped MnTe.[8] Below 300 K, the magnon lifetimes sharply increase by approximately five times. Interestingly, we observe no variations in paramagnon lifetimes in the deep paramagnetic regime above 500 K, despite the temperature-induced spin-crossover in Cr-doped MnTe. This suggests that paramagnon lifetime, and consequently paramagnon drag thermopower, is unaffected by temperature-driven spin-state

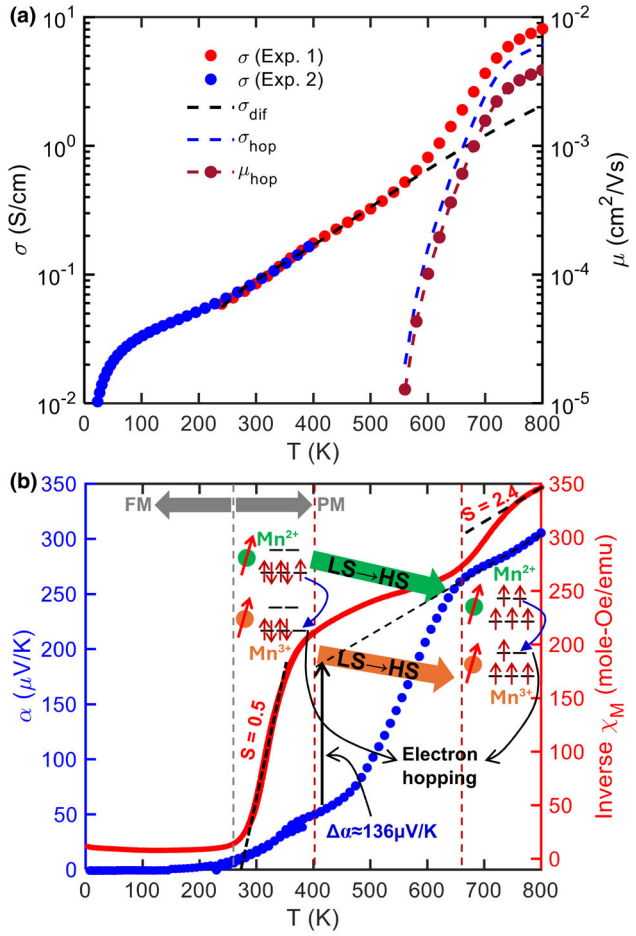


**Figure 3.** a) Electrical transport properties of 5% Cr-doped MnTe: Temperature-dependent electrical conductivity. Conductivity contributions from diffusion and hopping transport are estimated based on the dominant carrier transport mechanisms at different temperature ranges. The mobility of 5% Cr-doped MnTe in the hopping transport regime is estimated from the hopping conductivity contribution. b) Thermopower and Inverse Magnetic Susceptibility of 5% Cr-doped MnTe: Both thermopower and inverse magnetic susceptibility show enhancements in the paramagnetic regime. The changes in spin number occur within a similar temperature range, suggesting a significant influence of temperature-driven spin-crossover on the enhancement of paramagnetic thermopower. Data from 2 to 400 K and 300 to 800 K were collected using two different instruments, with an overlap in the 300–400 K range. Detailed experimental procedures are provided in the Materials and Methods section.

transitions. Therefore, the consistent paramagnon lifetime in Cr-doped MnTe implies that the anomalous enhancement of thermopower is not attributable to the paramagnon drag effect. However, a suppressed form of drag thermopower may still exist in Cr-doped MnTe due to its bipolar conduction nature.

It is worth mentioning that there is a distinction in the trends of anomalous thermopower enhancement between Li-doped and Cr-doped MnTe. In unipolar (p-type) Li-doped MnTe, the thermopower enhancement starts below the Néel temperature ($T_N = 307$ K), maximizes at $T_N$, and remains constant above $T_N$ at approximately 100 $\mu V K^{-1}$ up to ~900 K. Based on INS and heat capacity measurements, Li-doped MnTe has a sufficient paramagnon lifetime to contribute to the drag thermopower. In contrast, Cr-doped MnTe is a bipolar system with a significantly reduced drag thermopower. The extent of this reduction depends on carrier concentration, carrier effective mass, and magnon-carrier relaxation time.[17] In the ferromagnetic domain, the negligible thermopower in 5% Cr-doped MnTe suggests a nearly total cancelation of p-type and n-type drag and diffusion thermopower contributions due to the bipolar effect. In the paramagnetic domain, anomalous thermopower enhancement is observed only at ~500 K, while the magnetic transition occurs at ~280 K and the paramagnon lifetime remains almost constant throughout the entire paramagnetic domain. This implies that the underlying reason for thermopower enhancement in Cr-doped MnTe is different from that in Li-doped MnTe, as discussed in the following sections. The small enhancement in thermopower (~50 $\mu V K^{-1}$) at the beginning of the paramagnetic domain of Cr-doped MnTe could be due to paramagnon drag effects resulting from disproportionate changes in paramagnon properties for n-type and p-type carriers.

To validate the second prospective explanation for the anomalous behavior of paramagnetic thermopower, namely spin entropy, we need to understand the magnetic nature of Cr-doped MnTe in the paramagnetic regime. We have measured the magnetic susceptibility of Cr-doped MnTe to study the nature of magnetic ions (see Figure 3 [bottom]). The magnetic susceptibility reveals a spin-crossover occurring at the same temperature range where $Mn^{2+}$ and $Mn^{3+}$ ions transition from LS to HS states.[27] The Curie–Weiss analysis on magnetic susceptibility ($\chi_M$) of Cr-doped MnTe provides critical information about the spin states in the paramagnetic domain. In these domains, inverse susceptibility exhibits multiple slope changes associated with the change of the spin states. The spin number ($S$) is calculated from the inverse magnetic susceptibility using the Curie–Weiss law (see Ref. [17] for details on calculation), which is found as $S = 0.5$ at 300–400 K and $S = 2.4$ at >700 K. The $S = 0.5$ is due to the LS $Mn^{2+}$ ($LS^{Mn2+} = 0.5$) and $Mn^{3+}$ ions ($LS^{Mn3+} = 0$), while $S = 2.4$ is due to the HS states of $Mn^{2+}$ ($LS^{Mn2+} = 2.5$) and $Mn^{3+}$ ions ($LS^{Mn3+} = 2.0$). The magnetic susceptibility provides experimental evidence for temperature-driven spin crossover. It is also imperative to provide experimental support to spin entropy in Cr-doped MnTe, which can be achieved by studying different oxidation states of Mn ions.

To determine the oxidation states of Mn ions, we performed X-ray photoemission spectroscopy (XPS) on the powder sample. The sample holder was prepared inside a glovebox under an Ar environment by uniformly dispersing the powder on carbon tape and sealing the sample holder in an Ar-filled plastic bag to reduce the growth of native oxides. The sample holder was loaded into the XPS chamber under continuous nitrogen flow. The collected XPS spectrum of Mn ions is shown in **Figure 5**, along with the detected characteristic peaks associated with the Mn 2p cores. The entire XPS spectra are given in the File S1.

The obtained XPS features for Mn ions were analyzed with the CasaXPS software package to determine the existing oxidation states of Mn in Cr-doped MnTe. Binding Energy (BE) calibration was performed referencing the adventitious carbon peak (C 1s at 285.0 eV). The XPS spectra for Te 3d and Cr 2p cores have almost the same range of BE [File S1].[29] The peak fitting analysis for the Mn 2p core is illustrated in Figure 5. According to the analysis, XPS spectra of Mn 2p core can be deconvoluted into four peaks. The first two peaks are associated with $Mn^{2+}$ and $Mn^{3+}$ oxidation states, in agreement with the magnetic susceptibility results. The third peak can be associated with either $MnO_2$ or satellite features.[30,31] The oxide phase can originate from some native Mn oxides grown during the sample loading into the chamber. The fourth peak is the satellite peak originating from the charge transfer

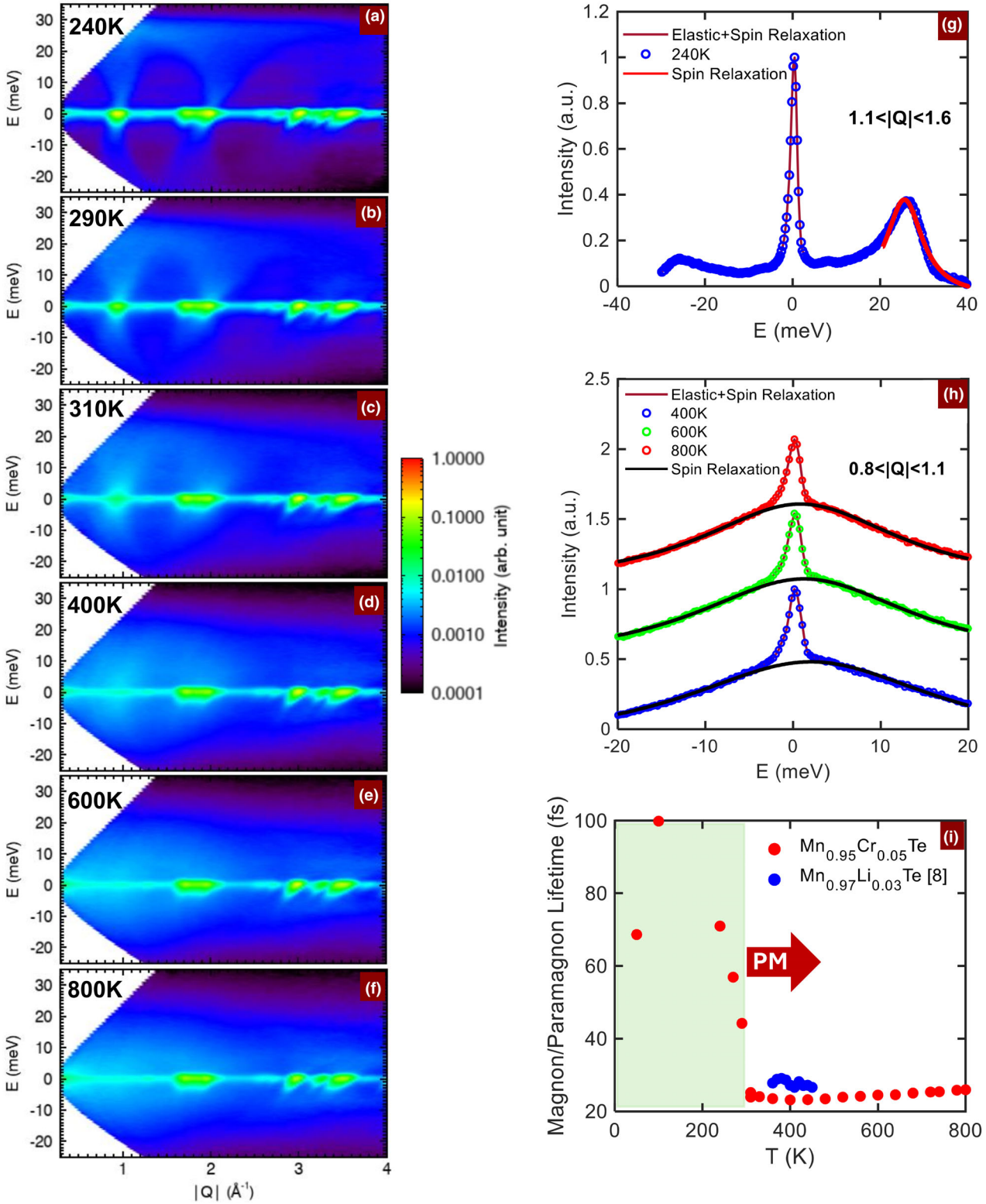


**Figure 4.** Inelastic neutron scattering spectra, *S(Q,E)*, for 5% Cr-doped MnTe at various temperatures within the magnetic (a, 240 K and b, 290 K) and paramagnetic domains (c, 310 K; d, 400 K; e, 600 K; and f, 800 K). g) Magnon bands in the magnetic domain are observed to broaden with increasing temperature. In the magnetic domain, spin-induced inelastic relaxation is quantified from the magnon branch in the range $1.1 < |Q| < 1.6$, distinct from the dominant elastic relaxation. h) In the PM domain, spin relaxation is determined by fitting the *S(E)* intensity within $0.8 < |Q| < 1.1$ to a Lorentzian profile. i) The resulting spin lifetime as a function of temperature is presented, alongside a comparison with the paramagnon lifetime reported in reference [8].

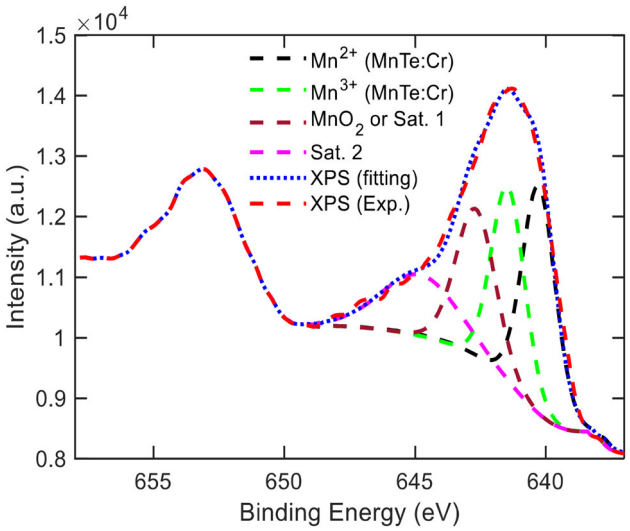


**Figure 5.** X-ray photoelectron spectroscopy (XPS) analysis of Mn 2p core levels in 5% Cr-doped MnTe, highlighting the peaks corresponding to $Mn^{2+}$ and $Mn^{3+}$ oxidation states.

between the outer electron shell of the ligand and the unfilled 3d shell of Mn during the XPS.[30,31] Combining the results of magnetic susceptibility and XPS, we found that Cr-doped MnTe has the presence of both $Mn^{2+}$ and $Mn^{3+}$ ions and spin-state transitioning happens at deep paramagnetic regime where the anomalous thermopower enhancement occurs. These findings support the spin-crossover mediated spin entropy thermopower concept which is discussed in the following section in detail.

## 3. Discussion

The spin entropy in 5% Cr-doped MnTe is primarily influenced by Mn ions, which are more prevalent than Cr ions. Susceptibility data indicates that Mn ions undergo a temperature-dependent spin-crossover above 400 K, a process governed by the balance between electron–electron repulsion energy (also known as chemical pressure) and the energy barrier imposed by crystal-field or spin-orbit coupling.[24] In Cr-doped MnTe, $Cr^{3+}$ ions, with their $3d^3$ configuration, maintain a HS state and generate a strong crystal field. This field, at low temperatures, keeps Mn ions in a LS state.[27] The carrier hopping associated with spin entropy in LS Mn ions can be amplified by a temperature-driven spin-crossover, which disrupts the spin-selection rule-controlled spin blockade effect.[18] Between the temperature range of 400–700 K, a gradual transition from LS to HS occurs. This slow transition also results in a broad peak in heat capacity in the paramagnetic domain, originating from the excess free energy due to the spin crossover.[27] In $d^n$ ($4 \leq n \leq 7$) transition metal systems, the coexistence of both LS and HS ions is possible when crystal field and Hund's exchange energy are comparable.[32] Table 2 summarizes the probable spin-states for Mn and Cr ions in Cr-doped MnTe, along with the allowed and forbidden spin transitions between $Mn^{3+}$ and $Mn^{2+}$, and $Cr^{3+}$ and $Cr^{2+}$ ions with different spin-states. The spin transitions in the system adhere to the selection or blockade rule, which stipulates that electron hopping to adjacent paramagnetic sites should result in an identical spin configuration, i.e., $\Delta m_s = 0$.[33]

**Table 2.** Overview of selection rules for spin transitions between $Mn^{3+}$/$Mn^{2+}$ and $Cr^{3+}$/$Cr^{2+}$ ions in Cr-doped MnTe.

| | HS $Mn^{2+}$ | LS $Mn^{2+}$ |
|---|---|---|
| HS $Mn^{3+}$ | ✓ | X |
| LS $Mn^{3+}$ | X | ✓ |
| | HS $Cr^{2+}$ | LS $Cr^{2+}$ |
| HS $Cr^{3+}$ | ✓ | X |
| LS $Cr^{3+}$ | X | ✓ |

In a 5% Cr-doped MnTe system, the spin entropy is primarily influenced by Mn ions, which are present in a significantly higher proportion (~95%) compared to Cr ions (~5%). This spin entropy arises from $Mn^{3+}$ and $Mn^{2+}$ ions in both LS and HS states, enabling electron hopping.

An unusual increase in PM thermopower is observed, which is attributed to the difference in spin entropy between LS and HS states of Mn ions. This difference is due to the varying spin degeneracy of Mn ions in these states.

The spin entropy contribution from Cr ions is negligible due to their limited presence. At the high-temperature limit, the thermopower due to orbital and spin degeneracy is expressed using the Heikes formula:[1,34]

$$\alpha_{SE} = -\frac{k_B}{e}\ln\left(g_c g_s\right) = -\frac{k_B}{e}\ln\left(\frac{g_2}{g_3}\frac{x}{1-x}\right) \tag{3}$$

Here, $g_c$ and $g_s$ represent the configurational and spin degeneracy of the magnetic ions, respectively. The spin degeneracy for Mn ions is defined as $g_3^{LS} = 3$ for $Mn^{3+}$ LS, $g_2^{LS} = 6$ for $Mn^{2+}$ LS, $g_3^{HS} = 25$ for $Mn^{3+}$ HS, and $g_2^{HS} = 6$ for $Mn^{2+}$ HS. The configurational degeneracy ($x$) remains constant in both LS and HS states. The transition between $Mn^{3+}$ and $Mn^{2+}$ from LS to HS alters the spin entropy, enhancing the thermopower. This can be calculated using the following relations:

$$\begin{aligned}\Delta\alpha_{SE} &= -\frac{k_B}{e}\ln\left(\frac{g_2^{HS}}{g_3^{HS}}\frac{x}{1-x}\right) + \frac{k_B}{e}\ln\left(\frac{g_2^{LS}}{g_3^{LS}}\frac{x}{1-x}\right) \\ &= -\frac{k_B}{e}\log\left(\frac{3}{25}\right) \approx 180\ \mu V\ K^{-1}\end{aligned} \tag{4}$$

The experimental results align with the observed anomalous enhancement of the PM thermopower, approximately $136\ \mu V\ K^{-1}$, considering experimental variations and approximating assumptions. The spin crossover-mediated spin entropy contribution significantly boosts thermopower by around 200%, electrical conductivity by approximately 280%, thermal conductivity by about 25%, and the thermoelectric figure of merit (zT) by roughly 655% [File S1].

However, despite these enhancements, the zT of 5% Cr-doped MnTe remains low (0.07 at around 800 K). This could potentially be improved by optimizing carrier hopping transport under the influence of spin-crossover mediated spin entropy.

It is important to note that while the thermopower and zT of Cr-doped MnTe show improvement, the bipolar nature of this material significantly restricts the overall thermoelectric performance of the system. The only advantage of this bipolar conduction nature is the ability to exclude the contribution of electronic and drag thermopower,

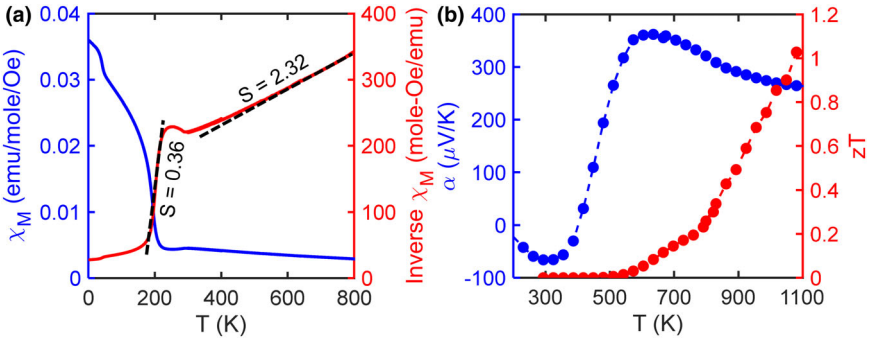


**Figure 6.** a) Depicts the magnetic susceptibility and its inverse for $Mn_{0.93}Cr_{0.04}Li_{0.03}Te$, providing evidence for the occurrence of spin-crossover within the paramagnetic domain. b) Presents the significant enhancement in thermopower and zT due to the influence of spin-crossover mediated spin entropy at approximately 350 K, culminating in a zT of approximately 1 at 1100 K.

thereby demonstrating the concept and advantage of spin-crossover mediated spin entropy in achieving higher thermoelectric performance. Given that the spin-crossover mediated spin entropy affects localized carriers, this concept could be leveraged to design a more efficient thermoelectric system with unipolar transport.

### 3.1. Enhancing zT through Optimization of Carrier Concentration and Cr Doping

The thermoelectric performance of Cr-doped MnTe can be enhanced by optimizing the Cr-doping and carrier concentration to maximize the spin-crossover mediated spin entropy gradient. Cr-doping in MnTe compensates for holes by replacing hole-donor Mn ions with electron-donor Cr ions. However, the hole concentration can be increased through Li-doping.[8]

X-ray diffraction (XRD) data of the Cr-doped MnTe samples reveal a small amount of CrTe, suggesting that not all Cr ions substitute Mn.[17] Interestingly, Li co-doping eliminates the CrTe, indicating a higher rate of Cr substitution and doping activation in the Li-doped MnTe system (see XRD analysis in Supporting Information). By optimizing Cr- and Li-doping, we can create a more efficient spin-driven thermoelectric system with a zT of approximately 1 at 1100 K.

**Figure 6a** presents the magnetic and inverse magnetic susceptibility of $Mn_{0.93}Cr_{0.04}Li_{0.03}Te$, supporting the occurrence of a temperature-driven spin-crossover. The magnetic susceptibility of both Cr-doped and Cr-Li co-doped MnTe exhibits similar temperature-dependent trends. $Mn_{0.93}Cr_{0.04}Li_{0.03}Te$ has a lower $T_C$ than $Mn_{0.95}Cr_{0.05}Te$, as the reduced amount of Cr creates less favorable conditions for the formation of FM Cr-Cr exchange interactions.[17] Furthermore, the spin crossover in $Mn_{0.93}Cr_{0.04}Li_{0.03}Te$ occurs at a lower temperature than in $Mn_{0.95}Cr_{0.05}Te$. The spin crossover temperature is influenced by the crystal field created by Cr ions and the exchange interaction between high-spin (HS) ions.[27] The lower quantities of Cr and Mn ions in $Mn_{0.93}Cr_{0.04}Li_{0.03}Te$ contribute to the shift of the spin crossover to a lower temperature.

The thermopower trends in Figure 6b corroborate the influence of spin entropy, which is augmented by the spin crossover in the PM domain. The zT for $Mn_{0.93}Cr_{0.04}Li_{0.03}Te$ reaches approximately 1 at 1100 K, a result of multiple factors including the optimized Fermi level and the effects of spin on both thermopower and electrical conductivity. The electrical and thermal conductivities are detailed in the File S1. At lower temperatures, the thermopower of $Mn_{0.93}Cr_{0.04}Li_{0.03}Te$ is negative, in contrast to the nearly zero thermopower of $Mn_{0.95}Cr_{0.05}Te$. This may seem counterintuitive since Cr ions act as electron donors in MnTe, which would typically lead to n-type conductivity.

The defect equations for CrLi-doped MnTe is as follows:

$$Mn_{0.93}Cr_{0.04}Li_{0.03}Te \rightarrow 0.03Li^{-}_{Mn} + 0.04Cr^{+}_{Mn} + 0.93Mn^{\times}_{Mn} + Te^{\times}_{Te} + 0.01e^{-} \quad (5)$$

As previously discussed, not all Cr ions are substitutionally doped into MnTe, resulting in a trace presence of CrTe in the Cr-doped MnTe. However, Li co-doping enhances the substitution of Mn by Cr, leading to a greater number of active electron donors and increased n-type conductivity in $Mn_{0.93}Cr_{0.04}Li_{0.03}Te$ compared to $Mn_{0.95}Cr_{0.05}Te$.

In general, the spin-crossover process enhances the spin-entropy-driven thermopower, and optimal doping improves the electrical conductivity, thereby increasing the zT of $Mn_{0.93}Cr_{0.04}Li_{0.03}Te$ to above 1 at high temperatures.

When compared to Li-doped MnTe, CrLi-doped MnTe exhibits lower thermoelectric performance; for instance, at approximately 900 K, CrLi-doped MnTe has a zT of about 0.5, whereas Li-doped MnTe reaches a zT of approximately 1.

It is important to note that the aim here is not to report a high-performing thermoelectric material system, but rather to demonstrate the potential of the spin-crossover driven spin-entropy effect in designing high-performance thermoelectrics. This is achieved through the synergistic optimization of other properties, highlighting the promising prospects of this approach.

## 4. Conclusion

As advancements in thermoelectric materials based on the optimization of electron and phonon transport properties begin to plateau, spin, and quantum materials have emerged as promising avenues for the development of high-performance thermoelectrics. A key challenge with conventional thermoelectrics is the inverse relationship between thermopower and carrier concentration, a consequence of electrons being fermions and thus subject to Fermi-Dirac statistics. In this study, we have introduced a new category of thermoelectric materials that can circumvent this fundamental limitation through the use of spin-crossover mediated spin entropy in the paramagnetic regime. This approach leads to a substantial increase in the thermoelectric power factor and zT. Specifically, for the case of simple binary material Cr-doped MnTe, the spin entropy and hopping transport boost the thermopower by approximately 200%, the electrical conductivity by around 280%, the thermal conductivity by about 25%, and the zT by roughly 655%. By further optimizing the sample in terms of carrier concentration and carrier hopping under the influence of the spin-crossover mediated spin entropy, the zT reaches unity at 1100 K. These findings introduce a new approach for the development of high-performance spin-driven thermoelectric materials, enabling the enhancement of thermopower without negatively impacting electrical

conductivity, thereby challenging traditional paradigms in thermoelectric material design.

## 5. Experimental Section

*Resource availability: Lead contact*—Further information and requests for resources should be directed to and will be fulfilled by the lead contact, Daryoosh Vashaee (dvashae@ncsu.edu).

*Materials availability*—This study did not generate new unique reagents.

*Materials and methods: Sample preparation*—The synthesis of Cr-doped and Cr-Li co-doped MnTe samples involved several steps, starting with the use of 99.99% pure Mn, Te, Cr, and Li elements. The elemental powders were first milled in a tungsten carbide (WC) bowl for 8 hours at 650 rpm under an argon environment, using a Fritsch P7PL planetary ball mill. Following this, the milled powder was annealed at 850 °C for 24 h under vacuum in a rocking furnace. This process ensured a homogeneous phase with a roughly uniform distribution of dopants. The annealed powder was then milled again for another 8 h in a WC bowl.

The powder was subsequently consolidated into cylindrical ingots using a homemade spark plasma sintering (SPS) system, housed in a glove box filled with argon. The SPS process was carried out under approximately 50 MPa pressure, with a constant heating rate of 60 °C/min, reaching a maximum temperature of 950 °C. This temperature was maintained for a soaking time of 20 min. Throughout the process, the levels of $O_2$ and $H_2O$ were consistently kept below 0.1 ppm inside the glove box. The resulting consolidated ingots achieved a density greater than 97% of the ideal value.

*Sample characterization*—The characterization of the Cr-doped and Cr-Li co-doped MnTe samples involved several techniques.

Firstly, room temperature *X-ray diffraction (XRD)* patterns were collected using a Rigaku Miniflex with Cu-Kα radiation at a wavelength of 0.154 nm, operating under 40 kV and 15 mA. The XRD analysis confirmed the polycrystalline phase of $Mn_{1-x}Cr_xTe$ without any phase impurity, with no traces of Cr, MnO, or $MnTe_2$ phases observed. The XRD pattern is provided in the Supporting Information.

The temperature-dependent *magnetic susceptibility* was measured using a vibrating sample magnetometer (VSM) in a Quantum Design DynaCool 12 T Physical Property Measurement System (PPMS). Measurements were taken from 2 to 400 K and from 300 to 800 K using the VSM Oven, all under a helium environment.

*Electrical conductivity* was determined using the standard 4-point probe method with Linseis equipment, from 200 to 850 K, also under a helium environment. Thermopower was measured simultaneously, with measurements performed for five different temperature gradients with a tight temperature tolerance. Each measurement was repeated four times and then averaged, with thermopower calculated from the slope fitting to five separate ΔT and ΔV.

A thin cylindrical disk (diameter 6 mm, thickness 0.65 mm) was cut from the ingot to measure the *thermal diffusivity* in the same direction as the electrical conductivity and thermopower. The thermal diffusivity was measured using the laser flash method with Linseis equipment under a vacuum environment, from 280 to 900 K. The *thermal conductivity* (κ) was calculated using the relation $\kappa = \rho C_p \upsilon$, where ρ is the mass density measured with the Archimedes method, and $C_p$ is the specific heat capacity.[27]

Low-temperature (2–400 K) *transport properties* were measured with the thermal transport option (TTO) puck of the Quantum Design DynaCool 12 T PPMS under zero field and a helium environment.

*Inelastic Neutron Scattering (INS)* measurements were performed with SEQUOIA, a direct geometry time-of-flight chopper spectrometer with fine energy transfer ($E$) and wave-vector ($Q$) resolution capabilities. Data were collected at a temperature range of 50–800 K with arbitrary step size (see Supporting Information). All data are represented as a function of neutron energy transfer, E, and momentum transfer, |Q|, where for elastically scattered neutrons $|Q| = 4\pi\sin(\theta)/\lambda$, with $\theta$ as the scattering angle and $\lambda$ as the neutron wavelength.

Lastly, the room-temperature *X-ray photoemission spectroscopy (XPS)* spectra were acquired using a FlexMod X-ray Photoelectron Spectrometer with a PHOIBOS 150 Hemispherical analyzer, offering a resolution of less than 1 eV. The XPS measurements and analysis were performed at the Analytical Instrumental Facility (AIF) at NC State University, under vacuum conditions with the base pressure in the $10^{-10}$ mbar range analysis chamber. The X-ray source for XPS measurement was Mg kα excitation with 1254 eV. The Takeoff angle was normal to the surface, while the X-Ray incidence angle was ∼30° from the surface and the X-ray source to the analyzer ∼60°. The XPS spectra were analyzed with the CasaXPS software package. The powder sample was uniformly dispersed on the sample holder with double-sided Carbon tape.

## Acknowledgements

The authors like to acknowledge the funding support by the National Science Foundation (NSF) under grant numbers CBET-2110603 and the Air Force Office of Scientific Research (AFOSR) under contract number FA9550-12-1-0225. This research used resources at the Spallation Neutron Source, a DOE Office of Science User Facility operated by the Oak Ridge National Laboratory. This work was partly performed at the Analytical Instrumentation Facility (AIF) at North Carolina State University, supported by the State of North Carolina and the National Science Foundation (award number ECCS-2025064).

## Conflict of Interests

The authors declare no competing interests.

## Authors Contributions

D.V. and M.M.H.P. proposed the concept and designed the experiment. M.M.H.P. and M.S. carried out the experiments and characterizations. M.S. and S.C. contributed to analyzing neutron scattering results, M.M.H.P. and D.V. analyzed the data, M.M.H.P. wrote the manuscript, and D.V. reviewed the manuscript.

## Data Availability Statement

The datasets generated in this study are available from the lead contact on reasonable request.

## Supporting Information

Supporting Information is available from the Wiley Online Library or from the author.

## Keywords

spin crossover, thermoelectric materials, thermopower enhancement, paramagnons, magnons

Received: March 2, 2024
Revised: May 23, 2024
Published online: June 12, 2024

[1] Y. Wang, N. S. Rogado, R. J. Cava, N. P. Ong, *Nature* **2003**, *423*, 425.
[2] P. M. Chaikin, G. Beni, *Phys. Rev. B* **1976**, *13*, 647.
[3] W. Koshibae, S. Maekawa, *Phys. Rev. Lett.* **2001**, *87*, 236603.
[4] W. Zhao, Z. Liu, Z. Sun, Q. Zhang, P. Wei, X. Mu, H. Zhou, C. Li, S. Ma, D. He, P. Ji, W. Zhu, X. Nie, X. Su, X. Tang, B. Shen, X. Dong, J. Yang, Y. Liu, J. Shi, *Nature* **2017**, *549*, 247.
[5] C. Li, S. Ma, P. Wei, W. Zhu, X. Nie, X. Sang, Z. Sun, Q. Zhang, W. Zhao, *Energ. Environ. Sci.* **2020**, *13*, 535.

[6] N. Tsujii, A. Nishide, J. Hayakawa, T. Mori, *Sci. Adv.* **2019**, *5*, eaat5935.
[7] T. Okabe, *J. Phys. Condens. Matter* **2010**, *22*, 115604.
[8] Y. Zheng, T. Lu, M. M. H. Polash, M. Rasoulianboroujeni, N. Liu, M. E. Manley, Y. Deng, P. J. Sun, X. L. Chen, R. P. Hermann, D. Vashaee, J. P. Heremans, H. Zhao, *Sci. Adv.* **2019**, *5*, eaat9461.
[9] M. M. H. Polash, F. Mohaddes, M. Rasoulianboroujeni, D. Vashaee, *J. Mater. Chem. C* **2020**, *8*, 4049.
[10] D.-J. Kim, K.-D. Lee, S. Surabhi, S.-G. Yoon, J.-R. Jeong, B.-G. Park, *Adv. Funct. Mater.* **2016**, *26*, 5507.
[11] H. Takaki, K. Kobayashi, M. Shimono, N. Kobayashi, K. Hirose, N. Tsujii, T. Mori, *Materials Today Phys.* **2017**, *3*, 85.
[12] M. Ikhlas, T. Tomita, T. Koretsune, M.-T. Suzuki, D. Nishio-Hamane, R. Arita, Y. Otani, S. Nakatsuji, *Nat. Phys.* **2017**, *13*, 1085.
[13] Z. Zamanipour, X. Shi, M. Mozafari, J. S. Krasinski, L. Tayebi, D. Vashaee, *Ceram. Int.*, **2013**, *39*, 2353.
[14] D. Vashaee, Y. Zhang, A. Shakouri, G. Zeng, Y. J. Chiu, *Phys. Rev. B*, **2006**, *74*, 195315.
[15] A. Gharleghi, M. M. H. Polash, R. Malekfar, S. A. Yamini, D. Vashaee, *J. Alloys Compd.* **2020**, *845*, 156188.
[16] A. Nikolaenko, J. von Milczewski, D. G. Joshi, S. Sachdev, *Phys. Rev. B* **2023**, *108*, 45123.
[17] M. M. H. Polash, D. Vashaee, *Phys. Rev. B* **2020**, *102*, 45202.
[18] A. Maignan, V. Caignaert, B. Raveau, D. Khomskii, G. Sawatzky, *Phys. Rev. Lett.* **2004**, *93*, 26401.
[19] D. P. Karim, A. T. Aldred, *Phys. Rev. B* **1979**, *20*, 2255.
[20] V. Vennelakanti, I. B. Kilic, G. G. Terrones, C. Duan, H. J. Kulik, *J. Phys. Chem.* **2024**, *128*, 204.
[21] J. D. Wasscher, C. Haas, *Phys. Lett.* **1964**, *8*, 302.
[22] P. Sun, K. R. Kumar, M. Lyu, Z. Wang, J. Xiang, W. Zhang, *Innovations* **2021**, *2*, 100101.
[23] S. Duan, Y. Yin, G.-Q. Liu, N. Man, J. Cai, X. Tan, K. Guo, X. Yang, J. Jiang, *Research (Wash DC)* **2021**, *2021*, 1949070.
[24] Y. Wang, Y. Sui, X. Wang, W. Su, W. Cao, X. Liu, *ACS Appl. Mater. Interfaces* **2010**, *28*, 2213.
[25] I. Terasaki, M. Iwakawa, T. Nakano, A. Tsukuda, W. Kobayashi, *Dalton Trans.* **2010**, *39*, 1005.
[26] S. Butt, W. Xu, W. Q. He, Q. Tan, G. K. Ren, Y. Lin, C. W. Nan, *J. Mater. Chem. A* **2014**, *2*, 19479.
[27] M. M. H. Polash, M. Rasoulianboroujeni, D. Vashaee, *Appl. Phys. Lett.* **2020**, *117*, 43903.
[28] M. M. H. Polash, D. Moseley, J. Zhang, R. P. Hermann, D. Vashaee, *Cell Rep. Phys. Sci.* **2021**, *2*, 100614.
[29] K. Shimada, T. Saitoh, H. Namatame, A. Fujimori, S. Ishida, S. Asano, M. Matoba, S. Anzai, *Phys. Rev. B* **1996**, *53*, 7673.
[30] R. J. Iwanowski, M. H. Heinonen, E. Janik, *Appl. Surf. Sci.* **2005**, *249*, 222.
[31] R. J. Iwanowski, M. H. Heinonen, B. Witkowska, *J. Alloys Compd.* **2010**, *491*, 13.
[32] R. A. Bari, J. Sivardidre, *Phys. Rev. B* **1972**, *5*, 4466.
[33] D. S. Negi, D. Singh, P. A. van Aken, R. Ahuja, *Phys. Rev. B* **2019**, *100*, 144108.
[34] W. Koshibae, K. Tsutsui, S. Maekawa, *Phys. Rev. B* **2000**, *62*, 6869.